



A FORMATION FLYING CONTROL ALGORITHM FOR THE CANX-4&5 LOW EARTH ORBIT NANOSATELLITE MISSION

Jesse K. Eyer^{a,*}, Christopher J. Damaren^a, Robert E. Zee^a and Elizabeth Cannon^b

^a*University of Toronto Institute for Aerospace Studies, 4925 Dufferin Street, Toronto, Ontario, Canada M3H 5T6*

^b*Department of Geomatics Engineering, 2500 University Drive NW, Calgary, Alberta, Canada T2N 1N4*

Abstract — The latest Canadian Advanced Nanospace eXperiment (CanX-4&5) is a dual-satellite formation flying demonstration mission. The mission objective is to prove that satellite formation flying can be accomplished with sub-meter tracking error accuracy for low ΔV requirements. The formation flying maneuvers for this mission require the development of control algorithms for autonomous formation maintenance and reconfiguration in the presence of orbital perturbations. In this paper, the development of suitable relative reference trajectories is discussed, and a linear quadratic regulator state-feedback solution for the control problem is described. A discrete thrusting scheme, using pulse width modulation, is applied to account for the fixed impulse limitation of the real spacecraft. A navigation algorithm uses Global Positioning System (GPS) carrier phase and Doppler data to obtain relative position and velocity measurements to within 2–5 cm and 1–3 cm/s, respectively. Using an extended Kalman filter, the estimated state of the spacecraft is formed by combining noisy GPS measurements with a simulated state. Four formations will be flown on the CanX-4&5 mission: two along-track orbit formations with spacecraft separation distances of 1000 and 500 m, and two projected circular orbit formations with separation distances of 100 and 50 m. The transition between each formation is achieved via a series of impulsive maneuvers performed by the deputy satellite. Current simulations of the overall mission—50 orbits in each formation—demonstrate submeter tracking errors during formation maintenance and a total required ΔV of 6.93 m/s. © 2008 Lister Science.

Keywords — Canadian Advanced Nanospace eXperiment, satellite formation flying, tracking error, nanosatellites

1. INTRODUCTION

Satellite formation flying is a challenging and innovative field that could potentially revolutionize the way in which many future satellite missions are conducted. The first interest in formation flying spacecraft arose during the NASA's Apollo Program, when missions required the Lunar Module and the Command Module to rendezvous on orbit from separations of more than 500 km. In modern times, formation flying is viewed as a potential way to decrease the cost of satellite missions while increasing their robustness. A formation of nano- or microsatellites could perform the same function as a single large satellite for a fraction of the cost. Moreover, should one satellite in the formation fail,

the remaining spacecraft could redistribute the tasks and continue the mission.

Although a great deal of theoretical research has been invested into the topic, very few missions have actually been slated to test formation flying in practice. The Gravity Recovery and Climate Experiment (GRACE) was launched in 2002, and operates in a low Earth orbit (LEO) with a 220 ± 50 km along-track spacecraft separation [1]. Its formation, however, is only loosely maintained via infrequent maneuvers executed from a ground station. Since then, NASA's A-Train, a series of six scientific satellites, was launched into a loose along-track formation to study various aspects of the atmosphere [2]. But, again, the control window for these satellites allows for only sparse maneuvers that can be performed from ground commands. Other experiments, such as the Demonstration of Autonomous Rendezvous Technology (DART) in 2005, have attempted to perform close proximity ma-

Updated version of paper IAC-07-B4.6.04 presented at the 58th International Astronautical Congress, in Hyderabad, India, September 24–28, 2007.

*Corresponding author. E-mail: eyer@utias.utoronto.ca.

neuers and rendezvous on-orbit, but have ultimately failed in their mission objectives [3]. A more recent mission, sponsored by the DLR, CNES, the Swedish Space Corporation, is PRIMA, set to launch at the end of 2008. PRIMA's goal is to demonstrate the use of Global Positioning System (GPS) guidance, navigation, and control algorithms for autonomous precision formation flying maneuvers, homing and rendezvous, proximity operations, and final approach/recede maneuvers. Although an ambitious project, PRIMA's controller design only enables the Main and Target satellites to control their relative positions to within ± 60 m [4].

The primary motivation of the CanX-4&5 mission is to demonstrate that satellite formation flying can be accomplished cheaply, precisely, and autonomously. As nanosatellites, CanX-4 and CanX-5 (CanX-4&5) will cost a mere fraction of the budget of other more elaborate missions, but will still achieve submeter position determination and control for modest fuel requirements (Fig. 1).

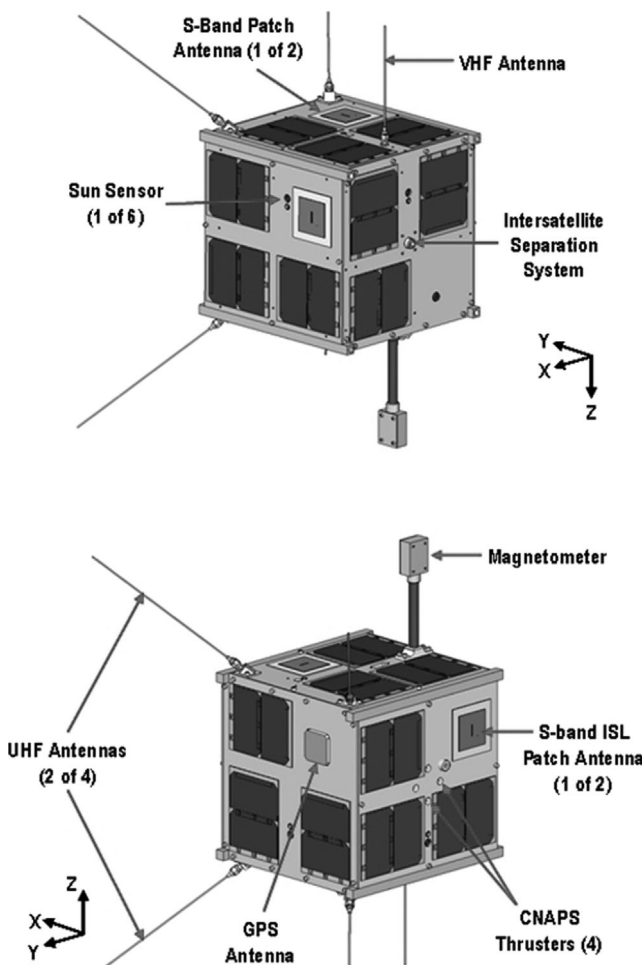


Fig. 1. CanX-4&5.

2. THE CANX-4&5 MISSION AND SUBSYSTEM REVIEW

The Canadian Advanced Nanospace eXperiment (CanX) program was established at the University of Toronto's Space Flight Laboratory (SFL) to develop leading-edge nanosatellite technology and to train graduate students in the design and construction of satellites via hands-on experience. The current satellites under development are CanX-4&5, two 7-kg, 20-cm cube nanosatellites that will demonstrate precise, automated formation flying maneuvers in LEO. On orbit, one satellite, designated the *deputy*, will perform regular thrusts to maintain the formation. The other satellite, the *chief*, will be free-floating and will be the point of reference for all relative motion.

The mission objectives require CanX-4&5 to fly 50 orbits in each of the four separate formations, to determine their relative positions to less than 10 cm, to control their relative positions to less than 1 m, and to accomplish all formation flying maneuvers using less than 14 m/s ΔV . To achieve these objectives, several key enabling technologies were developed, including an intersatellite separation system (ISS) (Fig. 2), a nanoscale propulsion system, a GPS-based navigation algorithm, a three-axis attitude determination and control system (ADCS), an intersatellite radio link, and a formation flying control algorithm.

2.1. Intersatellite Separation System

The CanX-4&5 nanosatellites will be launched and commissioned in a joined configuration. Upon completion of the commissioning phase, the satellites will disconnect and begin formation flying. To facilitate the linking and subsequent separation of the two satellites, an innovative ISS was designed [5]. The ISS

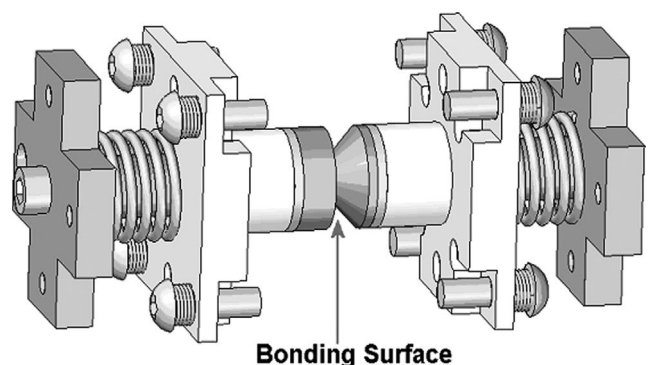


Fig. 2. The intersatellite separation system.

consists of two nearly identical halves, one mounted on the side of each satellite, with a spring-loaded cup/cone interface between them. This interface is coated in an electrically debonding agent, which, when hardened, acts as a rigid glue holding the satellites together. Once they are ready to separate, a small voltage is applied across the mechanism, which weakens the glue to the point where the springs overcome the adhesive force, breaking the bond and separating the two satellites. This separation sequence will impart a small ΔV to both satellites, allowing the deputy to drift to a suitable distance to begin formation flying.

2.2. Propulsion System

To maintain and transition between formations, the deputy satellite must thrust at regular intervals. The onboard propulsion system developed for CanX-4&5 is called the Canadian Nanosatellite Propulsion System (CNAPS) [5] (Fig. 3). CNAPS uses liquefied sulfur hexafluoride (SF_6) as a propellant and can achieve an ISP of approximately 35 s. With a fuel capacity of 300 ml, CNAPS is capable of a total ΔV of approximately 14 m/s.

Thrust is produced by four independently controlled thrusters in a cruciform configuration on one face of the satellite. Each thruster generates a constant thrust magnitude of 5 mN with a minimum impulse bit of 0.1 N s. Given this low thrust magnitude, it is occasionally necessary for CNAPS to thrust for extended periods.

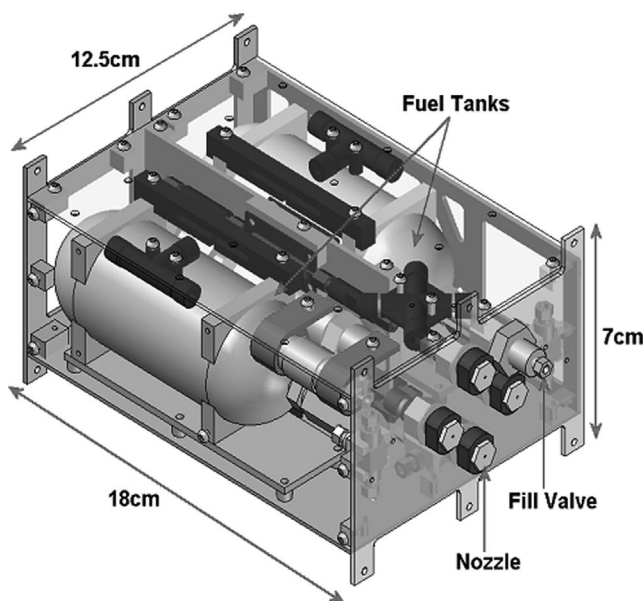


Fig. 3. The Canadian Nanosatellite Propulsion System.

Since each thruster can be calibrated independently, the four-thruster arrangement can be used to mitigate any unwanted torques generated during extended thrusts due to thruster misalignment.

2.3. GPS Navigation Algorithm

To obtain accurate absolute position and velocity measurements of the satellites, CanX-4&5 are each equipped with a NovAtel dual-band GPS receiver and an Aeroantenna dual-band GPS antenna. The GPS antennas are mounted on a face of each satellite orthogonal to its thrust axis, allowing it to retain some directional control over the antenna while the deputy thrusts in different directions. This control will be used to point the antenna as close to the zenith as possible in an effort to maximize the number of viewable GPS satellites.

Single-point GPS processing will allow each satellite to determine its absolute position to 2–5 m (RMS) and its absolute velocity to 5–10 cm/s (RMS). The Geomatics Group at the University of Calgary (U of C) have provided SFL with an algorithm that uses carrier phase and Doppler data with double differencing techniques to achieve relative position estimates to within 2–5 cm (RMS) and relative velocity estimates to within 1–3 cm/s (RMS) [5]. While the GPS receivers of both the deputy and the chief are locked onto the same four (or more) GPS satellites, the U of C algorithm will provide new absolute and relative position and velocity data to the formation flying algorithm every 5 seconds.

2.4 Attitude Determination and Control

With thrusters located only on one side of each spacecraft, it will be necessary to slew the satellites to a new attitude vector for each successive thrust during formation flying. To ensure that the same GPS satellites are kept in view, both the deputy and chief will simultaneously track the same attitude targets (although only the deputy will thrust).

The attitude determination sensors onboard CanX-4&5 consist of six coarse/fine sun sensors, a magnetometer, and three rate gyros. The combination of these sensor sets yields a pointing accuracy better than 1° [5]. Attitude actuation is provided via three orthogonally mounted reaction wheels (for fine pointing) and three magnetorquer coils (for detumbling and momentum dumping). The ADCS will be run on a dedicated onboard computer (OBC).

2.5. Intersatellite Link

Formation flying requires the chief and the deputy satellites to regularly exchange position, velocity, and attitude data. Therefore, it is necessary for CanX-4&5 to be equipped with an intersatellite link (ISL) S-band radio transceiver. Capable of transmitting/receiving 10 kbps to a maximum range of 5 km, the ISL has near omnidirectional coverage provided by identical patch antennas located on opposite sides of each spacecraft [5].

2.6. Formation Flying Algorithm

Both nanosatellites will be equipped with a dedicated OBC to run the formation flying control algorithm, dubbed FIONA (Formation flying Integrated Onboard Nanosatellite Algorithm). The principal objective of FIONA will be to regularly determine the tracking error of the deputy and to compute the optimal thrust necessary to correct this error. It will obtain relative position and velocity data from the U of C GPS algorithm and will output attitude target vectors to the ADCS computer and thruster on-times to the propulsion system.

3. FORMATION FLYING MISSION PLAN

Two formation types will be flown during the CanX-4&5 mission: along track orbit (ATO) formations and

projected circular orbit (PCO) formations. In the ATO formations, both satellites will essentially occupy the same orbit, but with one satellite leading the other by a particular separation distance. In the PCO formation, the satellites have slightly different inclination and eccentricity values so that, when viewed from Earth over the course of one orbit, the deputy appears to orbit the chief (Fig. 4).

Immediately after the commissioning phase, the ISS will separate the satellites, imparting a small ΔV onto both the deputy and chief in opposite directions. To ensure that the debonding adhesive breaks as anticipated, the ISS springs will have a compressive force of 70 N and deliver approximately 8 cm/s ΔV to each satellite. To achieve the starting conditions for the first formation (an ATO with a +1000 m intersatellite separation distance), however, requires only 2.6 cm/s ΔV in the negative along track direction. Therefore, the excess ΔV will be spent by separating the satellites partially in the orbit normal direction (Fig. 5). After one orbit, the deputy will perform a thrust to halt the separation and drop itself into the starting conditions for formation flying in a 1000-m ATO formation.

Over the course of the mission, formations will be flown in the following sequence: a 1000-m ATO, a 500-m ATO, a 50-m PCO, and a 100-m PCO. Each formation will be flown in station-keeping mode for 50 orbits (where one orbit around the Earth corresponds directly to one orbit of the deputy in the Hill frame). Upon completing each formation set, the deputy will perform a series of impulsive reconfiguration maneuvers to reach the next formation.

While the deputy will carry sufficient fuel to complete the entire mission alone, the chief will also fly

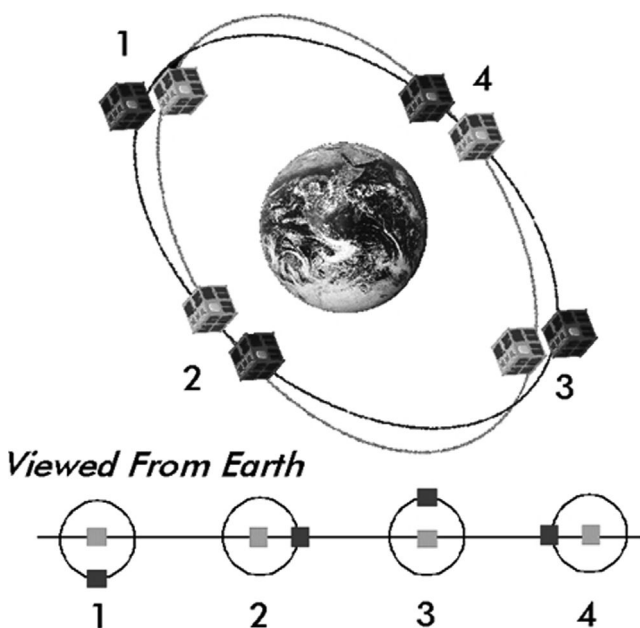


Fig. 4. CanX-4&5 in a projected circular orbit.

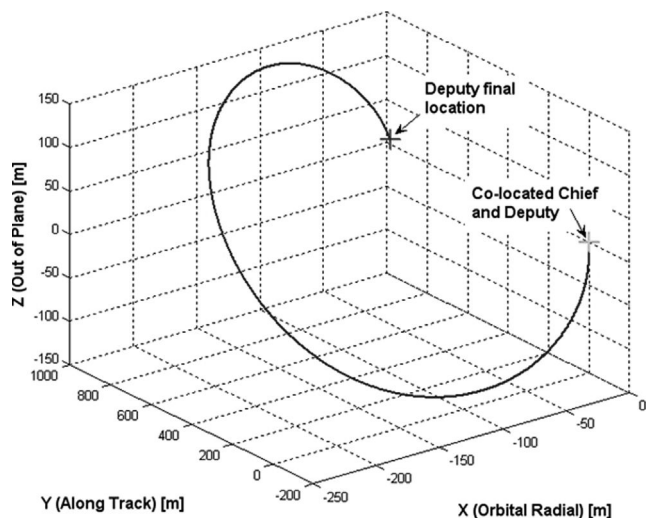


Fig. 5. Separation sequence for CanX-4&5.

with the same amount of fuel to ensure redundancy. Assuming the mission will be executed according to plan, following the main formation flying demonstration it should be possible for the chief and deputy to exchange roles to perform additional experiments. Such discretionary activities could include long duration formation flying (i.e., more than 100 orbits in a formation), inspection maneuvers, and J_2 -invariant formations for very long duration formation flying.

4. EQUATIONS OF MOTION

Orbital propagation of satellites is commonly conducted in the geocentric inertial (GCI) reference frame. For two spacecraft in a close formation, \underline{R}_c denotes the position of the chief, and \underline{R}_d denotes the position of the deputy, where $\underline{R} = [XYZ]^T$ is the GCI position of a generic satellite. The motion of these two satellites will evolve according to

$$\ddot{\underline{R}}_c = -\frac{\mu \underline{R}_c}{R_c^3} + \underline{F}(\underline{R}_c)_{\text{pert}} \quad (1)$$

$$\ddot{\underline{R}}_d = -\frac{\mu \underline{R}_d}{R_d^3} + \underline{F}(\underline{R}_d)_{\text{pert}} + \underline{u}_i \quad (2)$$

where μ is the geocentric gravitational constant, $\underline{F}(\underline{R})_{\text{pert}}$ is the perturbation force acting upon each satellite, and \underline{u}_i is the control force applied to the deputy during station-keeping maneuvers. In an LEO, the primary perturbing force is the J_2 gravitational harmonic effect due to the oblate shape of the Earth. Expressed in Cartesian coordinates, the J_2 force is

$$\underline{F}_{J_2}(\underline{R}) = -\frac{3\mu J_2 R_c^2}{2R^7} \begin{bmatrix} X^3 + XY^3 - 4XZ^2 \\ X^2Y + Y^3 - 4YZ^2 \\ 3X^2Z + 3Y^2Z - 2Z^3 \end{bmatrix} \quad (3)$$

where $J_2 = 1.0826269 \times 10^{-3}$ and R_c is the equatorial radius of the Earth. Higher order terms, J_3 – J_6 , play a smaller role,¹ but have also been added to FIONA's orbital propagator.

The dynamics of the two satellites can be concisely written by representing Eqs. (1) and (2) in state space form:

$$\dot{\underline{X}} = \underline{F}(\underline{X}) \text{ where } \underline{X} = \text{col}\{\underline{R}_c \ \dot{\underline{R}}_c \ \underline{R}_d \ \dot{\underline{R}}_d\} \quad (4)$$

¹Orbital simulations with Satellite Tool Kit (STK) have indicated that differential atmospheric drag will play only a small role as both satellites are identical and will match each other's attitudes at all times. Once the deputy has depleted most of its fuel, the difference in mass will give the satellites slightly different ballistic coefficients. The fuel margins on the mission, however, will handle the additional ΔV required to compensate for this small perturbation.

In formation flying applications, the relative position of the deputy with respect to the chief is expressed in the Hill frame, a local-vertical–local-horizontal (LVLH) reference frame that moves with the chief, and has its x -axis in the orbit radial direction, its y -axis in the velocity direction, and its z -axis in the orbit normal direction. The relative position of the deputy expressed in this frame is $\underline{r}_d = [x \ y \ z]^T$. This vector can be rotated into the GCI frame using the expression

$$\underline{r}_d = \underline{C}_{hi} [\underline{R}_d - \underline{R}_c], \quad \underline{C}_{hi}(t) = \begin{bmatrix} \frac{R_c}{R_c} & \frac{\underline{H}_c \times \underline{R}_c}{|\underline{H}_c \times \underline{R}_c|} & \frac{\underline{H}_c}{H_c} \end{bmatrix}^T \quad (5)$$

where \underline{C}_{hi} is the rotation matrix from the Hill frame (subscript h) to the GCI frame (subscript i), and $\underline{H} = \underline{R}_c \times \dot{\underline{R}}_c$ is the chief's angular momentum per unit mass. Figure 6 illustrates the GCI frame and the Hill frame.

4.1. Circular Reference Trajectories

During all station-keeping maneuvers, FIONA's control law will track a set of pre-established reference trajectories designed to yield periodic relative motion while closely matching the natural perturbed dynamics of the satellites. Although the actual relative dynamics of the deputy are nonlinear and nonperiodic, the Hill–Clohessy–Wiltshire (HCW) equations are linearized approximations of the full dynamics with periodic solutions [6]. They are given by Eqs. (6)–(8).

$$\ddot{x} - 2\omega\dot{y} - 3\omega^2x = 0 \quad (6)$$

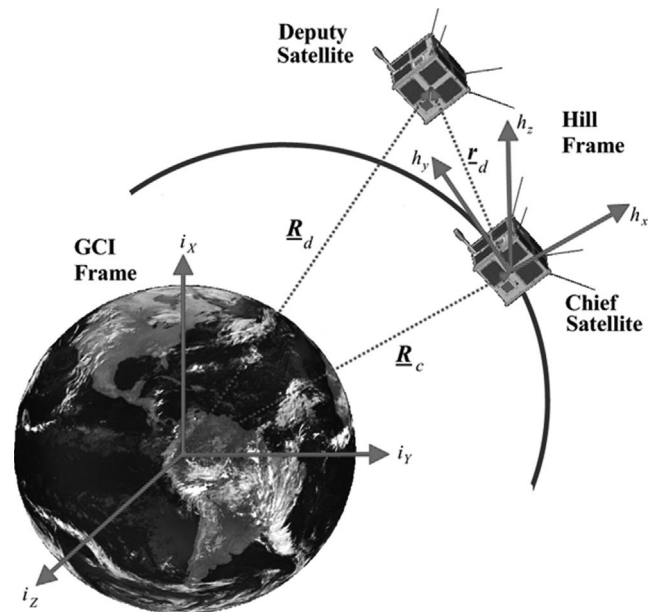


Fig. 6. The GCI and Hill reference frames.

$$\ddot{y} - 2\omega\dot{x} = 0 \quad (7)$$

$$\ddot{z} + \omega^2 z = 0 \quad (8)$$

where $\omega = \sqrt{\mu/R^3}$ is the circular orbital rate. Since the HCW equations assume the chief is in a circular orbit about the Earth and there are no perturbations acting on the satellites, their long-term predictive power is limited. Nevertheless, they are extremely useful for controller design and their solutions provide circular reference trajectories for the controller to track in the Hill frame. Their solutions are given by

$$x = \frac{c_1}{2} \sin(\omega t + \alpha) \quad (9)$$

$$y = c_1 \cos(\omega t + \alpha) + c_3 \quad (10)$$

$$z = c_2 \sin(\omega t + \alpha) \quad (11)$$

where α is the formation phase angle and the c_i 's are the constants of integration. Selecting $c_1 = c_2 = d_{\text{ref}}$ and $c_3 = 0$, where d_{ref} is the relative spacecraft separation distance, results in a PCO orbit of radius d_{ref} . Choosing $c_1 = c_2 = 0$, and $c_3 = d_{\text{ref}}$ results in an ATO formation.

4.2. Elliptical Reference Trajectories

The circular reference trajectories provide only a basic approximation of the natural perturbed relative motion of the deputy in the Hill frame. However, if the eccentricity of the chief's orbit is nonzero or if the separation between the two satellites increases (resulting in a linear increase in the differential J_2 perturbation), then the circular reference trajectories begin to break down, resulting in high ΔV and tracking error penalties. In such cases, better reference trajectories are provided by Lawden's elliptical equations of motion [7]. By selecting the constants of integration appropriately, it is possible to reduce the solutions to Lawden's equations into the reference trajectory expressions given by

$$x(\theta) = -d_1 \cos\theta \quad (12)$$

$$y(\theta) = \left[d_1 + \frac{d_1}{1 + \cos\theta} \right] \sin\theta + \frac{d_2}{1 + e \cos\theta} \quad (13)$$

$$z(\theta) = \left[\frac{d_3}{1 + e \cos\theta} \right] \cos\theta \quad (14)$$

where e is the orbital eccentricity, θ is the true anomaly, and the d_i 's are the constants of integration, chosen as follows: $d_1 = d_3 = 0$ and $d_2 = d_{\text{ref}}$ results in an ATO formation, and $d_1 = d_3 = d_{\text{ref}}$ and $d_2 = 0$ results in a PCO formation. Note that as $e \rightarrow 0$ these equations

collapse to the circular reference trajectories, but with a phase offset of $a = p/2$.

4.3. Calculating True Anomaly and Orbital Rate

It is apparent from Eqs. (12)–(14) that the elliptical reference trajectory position is a function of true anomaly θ , while the reference velocity will be a function of θ and the orbital rate, $\dot{\theta}$. Both of these values must be accurately computed to obtain a useful reference trajectory.

The most common method used to calculate θ takes a given time and solves Kepler's equation iteratively for the θ value at that time. However, because it is based on Keplerian dynamics, this method takes no orbital perturbations into consideration. Therefore, as the J_2 effect causes the perigee of the perturbed orbit to regress, there is a gradual divergence between the predictions of this method and reality. Using a θ value calculated by this method in an eccentric, perturbed orbit will induce instability in a state feedback control law. A better option is to calculate θ from the satellite's instantaneous state vector. Since the state will be affected by all orbital perturbations, this method accurately predicts the location of the spacecraft within its orbit and will result in a stable controller. The true anomaly is given by

$$\cos\theta = \frac{p - R}{R \cdot e} \quad (15)$$

$$\sin\theta = \frac{p(R \cdot V)}{h \cdot e \cdot R} \quad (16)$$

where p is the semilatus rectum, h is the magnitude of the angular momentum, and R is the norm of the position vector.

For an elliptical orbit, the orbital rate $\dot{\theta}$ is given by the expression

$$\dot{\theta} = \sqrt{\frac{\mu}{a^3}} \left(\frac{(1 + e \cos\theta)^2}{(1 - e^2)^{3/2}} \right) \quad (17)$$

Like the Keplerian method, however, this equation fails to take any orbital perturbations into consideration, and as a result gives a poor approximation of the orbital rate in a realistic orbital environment. FIONA obtains a much more accurate estimate of $\dot{\theta}$ by performing a simple backwards differencing method on θ every 5 s. Figure 7 compares the two methods over one orbit.

4.4. Formation-Based Reference Trajectory Selection

A drawback in using the state of the satellite to compute θ is that, as $e \rightarrow 0$, the elliptical reference tra-

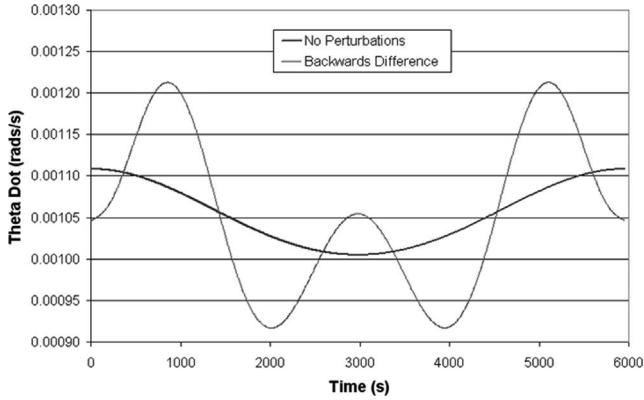


Fig. 7. Comparison of orbital rate calculation methods.

jectories begin to fail. The reason is quite clear from (15) and (16): since e is in the denominator of both expressions, they diverge as $e \rightarrow 0$. As a result, it is worth comparing the performance of each reference trajectory for each formation over the range of potential orbital eccentricities.

Anticipating a minimum perigee altitude of 550 km and a maximum apogee altitude of 900 km, the maximum orbital eccentricity of CanX-4&5 is not expected to exceed 0.025. For PCO formations at 50- and 100-m intersatellite separation distances, the circular reference trajectories outperform the elliptical reference trajectories for values of $e < 0.05$ (Fig. 8). Conversely, for ATO formations at 500- and 1000-m separation distances, the elliptical reference trajectories offer superior performance (Fig. 9).

The main factor influencing the performance of reference trajectories is the separation distance. Since the differential J_2 effect increases linearly with distance,

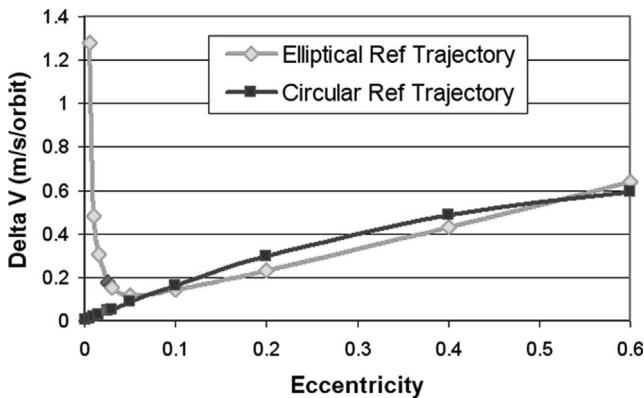


Fig. 8. 100 m PCO performance comparison between circular and elliptical reference trajectories as $e \rightarrow 0$.

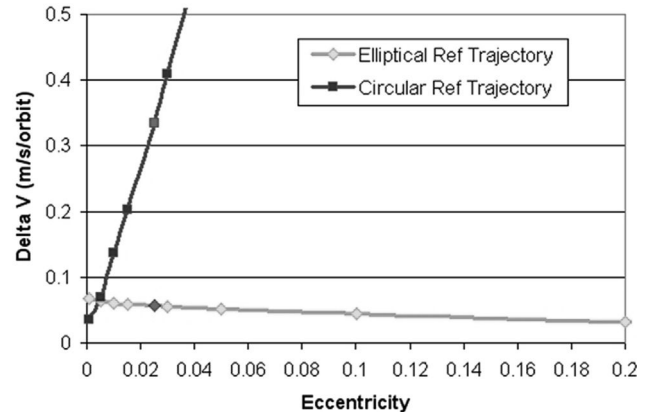


Fig. 9. 1000 m ATO performance comparison between circular and elliptical reference trajectories as $e \rightarrow 0$.

the deputy will experience greater perturbing forces in the ATO formations than in the PCO formations. In the presence of greater perturbation forces, the elliptical reference trajectories more closely match the natural perturbed motion of the satellite than the circular reference trajectories will, thus accounting for the improved performance of the elliptical trajectories at greater separation distances. Therefore, the CanX-4&5 deputy will track elliptical reference trajectories for both ATO formations and circular reference trajectories for both PCO formations.

5. STATE FEEDBACK CONTROL LAW

One of the principal challenges of a formation flying mission is to design a control law to actively mitigate orbital perturbations to the desired accuracy for modest ΔV requirements. The CanX-4&5 mission uses a linear state feedback control law with a gain matrix, \mathbf{K} , developed from a linear quadratic regulator (LQR) method. The first step in this method is to write the relative error dynamics in state space form:

$$\dot{\tilde{\mathbf{x}}} = \mathbf{A}_{\text{hill}} \tilde{\mathbf{x}} + \mathbf{B} \underline{u}_h \quad (18)$$

where $\tilde{\mathbf{x}} = \mathbf{x} - \mathbf{x}_{\text{ref}}$ is the relative state error vector ($\mathbf{x} = [x_d \ y_d \ z_d \ \dot{x}_d \ \dot{y}_d \ \dot{z}_d]^T$), \underline{u}_h is the control thrusts in the Hill frame, \mathbf{A}_{hill} is a matrix of the HCW dynamics given by Eqs. (6)–(8), and \mathbf{B} is the input matrix.

Next, an LQR method is used to find an input function $\underline{u}_h = f(\tilde{\mathbf{x}})$, such than the quadratic cost function

$$J = \int_0^{\infty} (\tilde{\mathbf{x}}^T \mathbf{Q} \tilde{\mathbf{x}} + \underline{u}_h^T \mathbf{R} \underline{u}_h) dt \quad (19)$$

is minimized for a given $\tilde{\mathbf{x}}$. The matrices \mathbf{Q} and \mathbf{R} represent the state cost and input cost, respectively, and can be weighted to yield tighter tracking of the reference trajectories for a higher ΔV cost, or vice versa. For the CanX-4&5 mission, \mathbf{Q} and \mathbf{R} are set to

$$\mathbf{Q} = \begin{bmatrix} \omega^2 & 0 & 0 & 0 & 0 & 0 \\ 0 & \omega^2 & 0 & 0 & 0 & 0 \\ 0 & 0 & \omega^2 & 0 & 0 & 0 \\ 0 & 0 & 0 & 1 & 0 & 0 \\ 0 & 0 & 0 & 0 & 1 & 0 \\ 0 & 0 & 0 & 0 & 0 & 1 \end{bmatrix} \quad \mathbf{R} = \frac{0.01}{\omega^2} \begin{bmatrix} 1 & 0 & 0 \\ 0 & 1 & 0 \\ 0 & 0 & 1 \end{bmatrix} \quad (20)$$

The optimal control law for Eq. (19) is given by the linear state-feedback formula

$$\mathbf{u}_h = -\mathbf{R}^{-1}\mathbf{B}^T\mathbf{P}\tilde{\mathbf{x}} = -\mathbf{K}\tilde{\mathbf{x}} = -\mathbf{K}(\mathbf{x} - \mathbf{x}_{\text{ref}}) \quad (21)$$

where \mathbf{K} is the controller gain matrix and \mathbf{P} is a matrix found by algebraically solving the Riccati equation. Finally, \mathbf{u}_h is rotated into the GCI frame and applied to the spacecraft states in Eq. (4), which the onboard propagator then integrates using a fixed-step fourth-order Runge–Kutta method to predict the dynamics of both spacecraft.

6. PULSE WIDTH MODULATION THRUSTING STRATEGY

Since the CanX-4&5 nanosatellite thrusters will produce a constant thrust of 5 mN, it is necessary to implement the corrective thrusts via a pulse width modulation (PWM) strategy. With PWM, the magnitude of the thrust remains constant while the thruster on time (t_{on}) is varied. At the beginning of each PWM cycle, the thruster on time is computed from the following equation:

$$t_{\text{on}} = \frac{|\mathbf{u}|}{U_{\text{max}}} T_{\text{PWM}} \quad (22)$$

where $|\mathbf{u}|$ is the magnitude of the control forces computed from the state feedback law (in Eq. (21)), U_{max} is the maximum thrust per unit mass from the CNAPS thrusters, and T_{PWM} is the PWM period for CanX-4&5. A unit vector in the direction of the thrust is next calculated via the equation

$$\mathbf{a}_{\text{thrust}} = \frac{\mathbf{u}}{|\mathbf{u}|} \quad (23)$$

Finally, the corrective thrust is from

$$\mathbf{u}_{\text{PWM}} = U_{\text{max}} \mathbf{a}_{\text{thrust}} \quad (24)$$

This thrust is applied to the deputy's dynamics (in Eq. (2)) and the model is propagated for the duration of

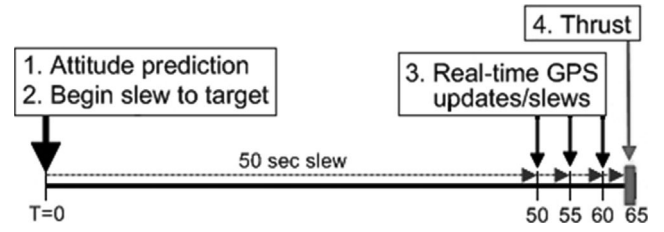


Fig. 10. ACS prediction technique.

the thrust. The PWM technique is only valid for T_{PWM} values small enough to approximate the continuous dynamics of the system; above 155 s, the approximation breaks down and the discrete thrusting scheme becomes unstable. A PWM period of 65 s has been selected for the CanX-4&5 mission, well away from the instability.

6.1. Attitude Prediction

Unfortunately, the conventional PWM theory works quite poorly on a real spacecraft. Once the calculation to determine the thrust direction and on time is complete, it takes a finite amount of time to actually slew the spacecraft to that attitude and perform the thrust. As a result, by the time the spacecraft is ready to thrust, it has drifted in its orbit and the original attitude target is no longer valid. Calculating at the start of the PWM period, slewing, and then thrusting at the end cycle incurs high ΔV and tracking error penalties, directly proportional to the length of the PWM period.

To overcome this problem, FIONA uses an attitude prediction technique. At the beginning of each 65-s PWM period, the state of the two satellites is propagated open loop forward in time by 50 s and the at-

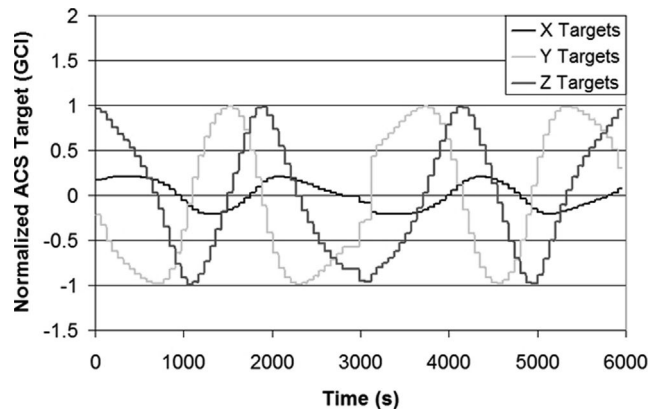


Fig. 11. 1000 m ATO attitude target vectors.

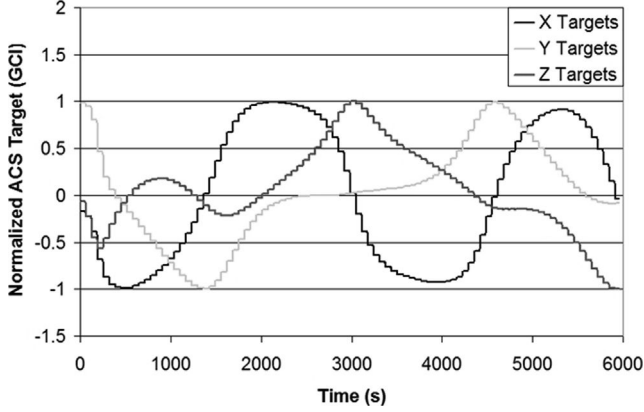


Fig. 12. 100 m PCO attitude target vectors.

attitude target vector is acquired for this time (from Eq. (23)). This target is then passed to the ACS computer that instructs the deputy to slew to this attitude over the next 50 s. Upon achieving this target, FIONA uses real-time GPS data to perform attitude target updates/slews every 5 s to readjust the attitude up until the thrust. A schematic of this method appears in Fig. 10.

The attitude target vectors sent to the ACS computer are set in the GCI frame and are depicted over one orbit in Fig. 11 for a 1000-m ATO formation and Fig. 12 for a 100 PCO formation. Note that the targets do not appear periodic. This is due to the fact that, at $t = 0$, the deputy is located at the initial conditions for that specific reference trajectory, and has not yet settled into its controlled limit cycle.

7. GUIDANCE AND NAVIGATION

One of the key elements in formation flying is the accurate determination of the constituent satellites' position and velocity. The CanX-4&5 mission uses a NovAtel GPS receiver and an Aeroantenna GPS antenna, in combination with the U of C's algorithm, to provide highly accurate position and velocity data to FIONA in both the GCI and Hill reference frames. Two measurements are of particular importance: the absolute state of the chief, which is used for all rotation matrices from GCI to the Hill frame and vice versa (Eq. (5)); and the relative state of the deputy, which is used in the control feedback loop (\underline{x} in Eq. (21)). To acquire this data under nominal operating conditions, both the chief and the deputy must have a lock on four or more of the same GPS satellites. Because the attitude target vectors required for formation flying often demand the satellites to rapidly slew to a new pointing direction, CanX-4&5's receivers

will frequently lose their lock on the mandatory 4+ GPS satellites. Further complicating the issue is the fact that the NovAtel receivers have a warm start time of ~ 30 s to reacquire lock. Satellite Tool Kit (STK) simulations have indicated that these "GPS blackout" scenarios will occur between 20 and 50 times per orbit with durations ranging from 5 to 360 s.

To continue the formation flying experiment during GPS blackouts, an extended Kalman filter (EKF) and an orbital propagator were added to FIONA. The EKF is synchronized with the GPS data refresh rate at 5-s intervals. During the *time update* phase of the filter at step i , the covariance matrix \mathbf{P}_i^- is assembled based on a state transition matrix \mathbf{F}_i (developed from the orbital dynamics of Eqs. (1) and (2)), and a process noise covariance matrix, \mathbf{Q}_i [8]

$$\mathbf{P}_i^- = \mathbf{F}_i \mathbf{P}_{i-1}^+ \mathbf{F}_i^T + \mathbf{Q}_i \quad (25)$$

During the *measurement update* phase, the inertial state estimate $\hat{\mathbf{X}}_i^+$ is obtained and the error covariance matrix is updated.

$$\begin{aligned} \mathbf{K}_i &= \mathbf{P}_i^- \mathbf{H}_i^T (\mathbf{H}_i \mathbf{P}_i^- \mathbf{H}_i^T + \mathbf{R}_i)^{-1} \\ \hat{\mathbf{X}}_i^+ &= \hat{\mathbf{X}}_i^- + \mathbf{K}_i (\mathbf{z}_i - \mathbf{h}_i) \\ \mathbf{P}_i^+ &= (\mathbf{I} - \mathbf{K}_i \mathbf{H}_i) \mathbf{P}_i^- (\mathbf{I} - \mathbf{K}_i \mathbf{H}_i)^{-1} + \mathbf{K}_i \mathbf{R}_i \mathbf{K}_i^{-1} \end{aligned} \quad (26)$$

where \mathbf{K}_i is the Kalman gain matrix, \mathbf{R}_i is the measurement noise covariance, \mathbf{H}_i is the local observation matrix, \mathbf{z}_i is the GPS position measurement, and \mathbf{h}_i is the estimated position.

During GPS lock, measurements from the GPS receiver and the U of C algorithm are used in FIONA directly. Moreover, the EKF combines these measurements with the output of the onboard orbital simulator to produce an accurate, noise-free estimated state of both satellites. This EKF estimation then becomes the input for the orbital propagator during the next time step, and thus it serves to keep the orbital propagator accurate and up to date. Figure 13 illustrates the data flow within the formation flying simulation environment during GPS lock.

During GPS blackout, when one or both satellites is locked onto fewer than four GPS satellites, FIONA bypasses the U of C algorithm and simply propagates the last known EKF update through the onboard orbital propagator (Fig. 14). The formation flying experiment can, therefore, continue for short periods until GPS lock has been reestablished. STK tests have shown that when FIONA operates on an orbital propagator with J_2 - J_6 gravitational perturbations, the deputy will drift less than 40 cm over the course of a 360-s blackout.

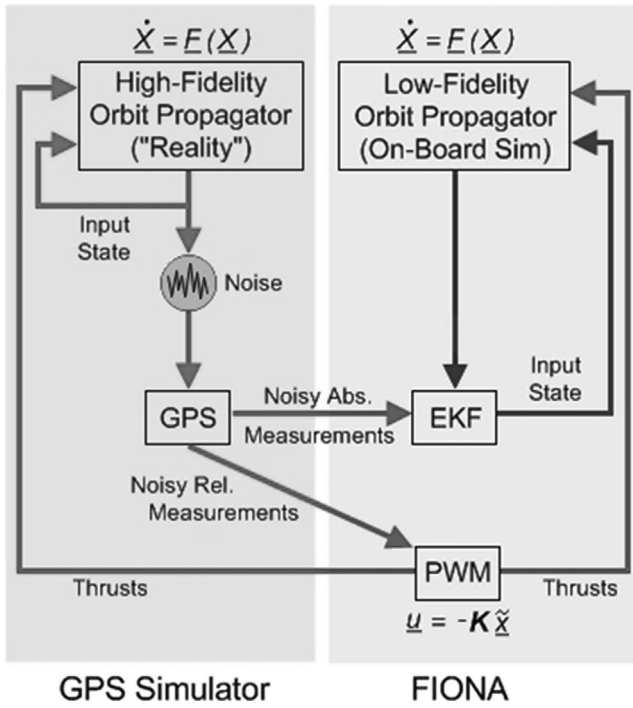


Fig. 13. Data flow within the formation flying simulation environment during GPS lock.

7.1. GPS Measurement Noise Mitigation

As previously noted, the GPS measurements are noisy. Single-point absolute position and velocity measurements are accurate to 2–5 m (RMS) and 5–10 cm/s (RMS), respectively, while the relative measurements provided by the U of C algorithm are accurate to 2–5 cm (RMS) and 1–3 cm/s (RMS). In the formation flying simulation environment, this noise is modeled as scaled Gaussian white noise applied separately to each channel (chief's x -position, chief's y -position, etc.). By tuning the EKF to reduce the dependence on the GPS measurements (and give a correspondingly greater emphasis on the orbital propagator output), it is possible to filter out much of the noise while still retaining their corrective influence over the EKF state estimate. Such a reduced dependence on the GPS measurements also helps prevent sensor spikes when transitioning in and out of blackouts, and to reduce the noise on the attitude target vectors.

While the LQR controller is robust to noise on the absolute chief state (which translates to noise in the rotation matrices from GCI to the Hill frame and vice versa) and robust to noise on the deputy's relative position measurements, it is *highly* sensitive to noise on the relative velocity measurements. Figure 15 illustrates increase in tracking error due to increasingly noisy velocity measurements. Even a velocity noise of

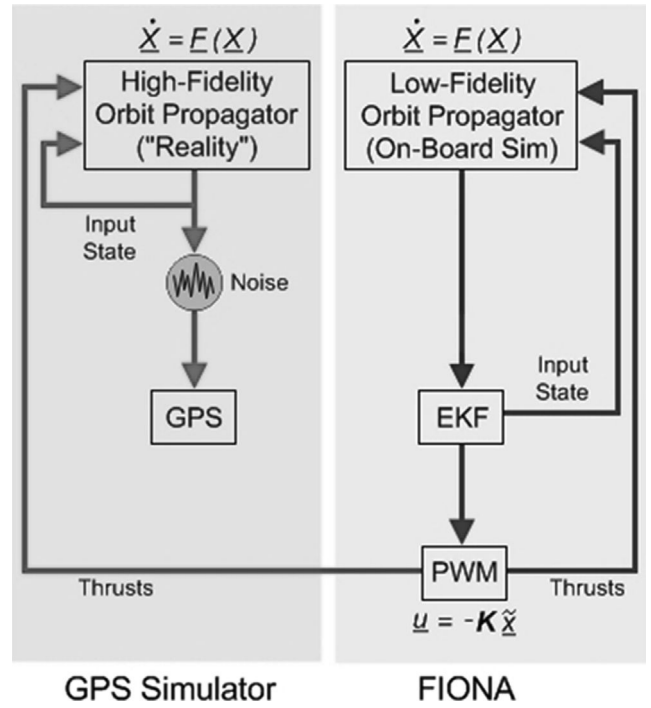


Fig. 14. Data flow within the formation flying simulation environment during GPS blackout.

0.0027 m/s (RMS) causes the tracking error to exceed the 1 m requirement.

Several methods were explored for handling the relative velocity noise in the state-feedback control loop. The technique that yields the best performance is an unconventional hybrid control strategy. The controller continues to use the state feedback control law of Eq. (21), but the deputy's real relative state (x) is redefined as follows:

$$\mathbf{x} = [x_{\text{GPS}}, y_{\text{GPS}}, z_{\text{GPS}}, V_{x_{\text{EKF}}}, V_{y_{\text{EKF}}}, V_{z_{\text{EKF}}}]^T \quad (27)$$

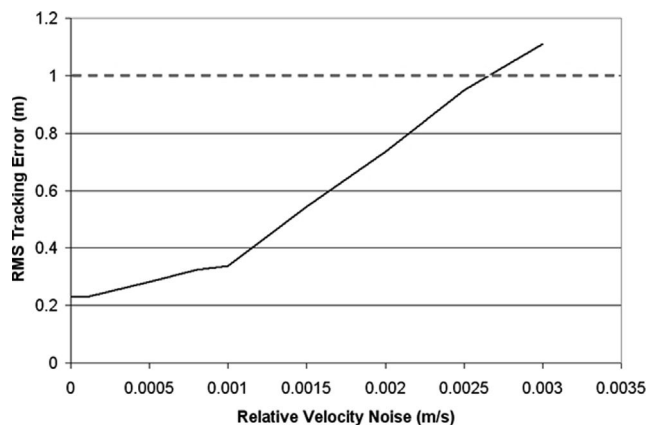


Fig. 15. Relative velocity measurement noise.

The relative position values are still obtained from the noisy GPS measurements, but the relative velocity values are based from the latest EKF estimate rotated into the Hill reference frame. Since the EKF places more emphasis on the simulated states, its state estimate is mostly noise-free. But since it is still updated every 5 s by GPS measurements, it remains very accurate. Because there is no longer any dependence on the noisy relative GPS velocity measurements, the results exhibit excellent ΔV and tracking error characteristics.

8. RECONFIGURATION MANEUVERS

One of the primary challenges of the CanX-4&5 mission is to ensure fuel-efficient and accurate reconfiguration maneuvers between each formation. Although an impulsive thrusting scheme based on the HCW equations was identified by Vaddi et al. [9], the method incurs large overshoot errors (14–74 m) when subjected to an elliptical orbit, gravitational perturbations, and nonimpulsive thrusting.

An improved method has been developed for the CanX-4&5 mission that minimizes the overshoot error for reconfiguration maneuvers in realistic orbital environments. It uses the analytical solution to a state space model

$$\begin{aligned} \mathbf{x}(t) &= e^{\mathbf{A}t}\mathbf{x}(0) + \int_0^t e^{\mathbf{A}(t-\tau)}\mathbf{B}\underline{\mathbf{u}}(\tau)d\tau \\ &= \mathbf{F}(t)\mathbf{x}(0) + \mathbf{B}_1\hat{\mathbf{u}}_1 + \mathbf{B}_2\hat{\mathbf{u}}_2 \end{aligned} \quad (28)$$

where \mathbf{x} is the relative state, \mathbf{A} is a matrix with the HCW dynamics, \mathbf{B} is the input matrix, $\underline{\mathbf{u}}$ is a vector containing the elements from both thrusts, $\mathbf{B}_i = \mathbf{F}(t - t_i)\mathbf{B}$ and where $\mathbf{F}(t)$ is the state transition matrix based on the HCW equations, given by

$$\mathbf{F}(t) = \begin{bmatrix} 4 - c & 0 & 0 & s/\omega & 2(1 - c)/\omega & 0 \\ 6(s - \omega t) & 1 & 0 & -2(1 - c)/\omega & (4s - 3\omega t)/\omega & 0 \\ 0 & 0 & c & 0 & 0 & s/\omega \\ 3\omega s & 0 & 0 & c & 2s & 0 \\ -6(s - \omega t) & 0 & 0 & -2s & 4c - 3 & 0 \\ 0 & 0 & -\omega s & 0 & 0 & c \end{bmatrix} \quad (29)$$

where $s = \sin(\omega t)$ and $c = \cos(\omega t)$. Eq. (28) can be rearranged to solve for the thrust vectors $\hat{\mathbf{u}}_1$ and $\hat{\mathbf{u}}_2$ necessary to reconfigure the deputy satellite between relative states (Fig. 16).

Alone, the state transition matrix method has a limited accuracy due to the linearized HCW dynamics. Moreover, its accuracy is highly dependent on *when* the two thrusts are performed. As such, it is possible to

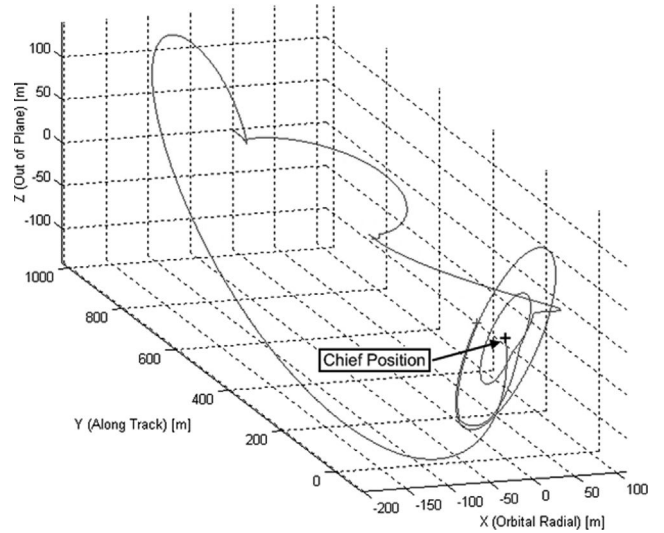


Fig. 16. The relative motion of the deputy with respect to the chief for the full mission profile.

pose the STM (State Transition Matrix) method as an optimization problem to mitigate the overshoot errors and reduce the ΔV requirements of the reconfiguration maneuvers. The thrust start times are selected as design variables. The STM uses these to calculate the thrust vectors, which are sent through a high-fidelity orbital propagator to determine the thruster on-times and overshoot errors. A gradient-based SQP optimization method is used to minimize the overall on-time of the thrusts (corresponding to minimizing the ΔV) for tight overshoot error constraints (<2.5 m for each position error, and <0.1 m/s for each velocity error). The process worked to greatly reduce the overshoot error, but in general required longer thruster on-times than the method described in [9]. The overall increase in ΔV for the three reconfiguration maneuvers is approximately 6.5 cm/s, well within the fuel margins for CanX-4&5. The results of the reconfiguration maneuvers are summarized in Table 1. A full discussion of the STM optimization method is presented in [10].

9. FORMATION FLYING SIMULATION RESULTS

The flight code for FIONA was written in C and wrapped in a real-time Simulink environment, which could simulate noisy GPS measurements, thrust direction, and magnitude errors, etc. The entire mission (separation sequence, four formations, and the associated reconfiguration maneuvers) was simulated, and the results are presented in Table 1 on a per orbit basis. The tracking error for each formation is <25 cm (RMS), well beneath the 1 m tracking accuracy required for the

Table 1
Formation flying simulation summary

Formation	ΔV (m/s)	Tracking/overshoot error (m)
Separation	0.1017	6.81
1000 m ATO	0.0595	0.236
ATO \rightarrow ATO	0.0880	3.68
500 m ATO	0.0299	0.127
ATO \rightarrow PCO	0.1204	3.29
50 m PCO	0.0138	0.110
PCO \rightarrow PCO	0.0849	3.49
100 m PCO	0.0275	0.0165

mission. Given 50 orbits in each formation, the mission is predicted to require ~ 6.93 m/s in ΔV , well below the 14.22 m/s available on each satellite.

10. CONCLUSION

CanX-4&5 is a nanosatellite formation flying demonstration mission that will validate several key technologies, including formation flying guidance and control algorithms. The mission will also prove that formation flying can be accomplished for a modest budget, yet still achieve submeter position determination and control. This paper reviews the mission and the technologies essential for formation flying, and discusses FIONA, the formation flying algorithm at length.

FIONA uses an LQR state feedback control law that has been modified to account for noise on the GPS relative velocity measurements. The controller tracks circular reference trajectories for the 1000- and the 500-m ATO formations, and elliptical reference trajectories for the 50- and 100-m PCO formations. An impulsive reconfiguration plan, based on an optimized state transition matrix method, is used to transition the deputy from each formation to the next. A PWM thrusting scheme with a period of 65 s was developed to account for the constant 5 mN force from CanX-4&5's CNAPS thrusters, and a prediction method was used to determine accurate attitude target vectors in advance of each thrust. An algorithm provided by the U of C uses GPS measurements to calculate the relative position and velocity of each satellite to within 2–5 cm and 1–3 cm/s, respectively. In GPS blackout scenarios, an EKF will provide the onboard orbital propagator with an accurate estimate of the satellites' last known state, allowing the formation flying experiment to continue until GPS lock is reestablished. Simulations of the overall mission indicate submeter tracking for the

formation maintenance component of the mission and a total ΔV of approximately 6.93 m/s.

The CanX-4&5 mission will be among the first spacecraft to demonstrate fully autonomous precision formation flying, and will set the stage for all future LEO formation flying missions.

ACKNOWLEDGMENTS

The authors gratefully acknowledge the ongoing contributions of the CanX student team: Norman Deschamps, Jonathan Gryzmisch, Liam O'Brian, Adam Philip, Chris Short, and Maria Short. In addition, the authors wish to thank the SFL staff for their support: Alex Beattie, Stuart Eagleson, Cordell Grant, Daniel Kekez, Stephen Mauthe, Freddy Pranajaya, and Tarun Tuli.

REFERENCES

- [1] Kirschner, M., Montenbruck, O., Bettadpur, S., Flight dynamics aspects of the GRACE formation flying, *2nd International Workshop on Satellite Constellations and Formation Flying Proceedings*, Technion, Israel Inst. of Technology, Haifa, Israel, Feb. 2001, pp. 187–194.
- [2] Folta, D. and Hawkins, A., Preliminary Results of NASA's First Autonomous Formation Flying Experiment Earth Observing-1 (EO-1), NASA Goddard Flight Center, Greenbelt, MD, 2001, pp. 1–21.
- [3] Overview of the DART Mishap Investigation Results (online NASA report), http://www.nasa.gov/pdf/148072main_DART_mishap_overview.pdf.
- [4] Gill, E., D'Amico, S., Montenbruck, O., Autonomous Formation Flying for the PRISMA Mission, 16th AAS/AIAA Space Mechanics Meeting, Tampa, FL, 2006.
- [5] Orr, N., Eyer, J., Larouche, B. and Zee, R., Precision formation flight: the CanX-4 and CanX-5 dual nanosatellite mission, 21st AIAA/USU Conference on Small Satellites, Salt Lake City, UT, August 2007.
- [6] Schaub, H. and Junkins, J.L., Analytical mechanics of space systems, AIAA, 2003, pp. 593–602.
- [7] Inalhan, G., Tillerson, M. and How, J.P., Relative dynamics and control of spacecraft formations in eccentric orbits, *Journal of Guidance, Control, and Dynamics*, **25**(1), pp. 48–59, January–February 2002.
- [8] Leung, W. and Damaren, C. J., A Comparison of the pseudo-linear and extended Kalman filters for spacecraft attitude estimation, AIAA Guidance, Navigation, and Control Conference and Exhibit, Rhode Island, Aug. 2004.
- [9] Vaddi, S.S., Alfriend, K.T., Vadali, S.R. and Sengupta, P., Formation establishment and reconfiguration using impulsive control, *Journal of Guidance, Control, and Dynamics*, **28**(2), 262–268, March–April 2005.
- [10] Eyer, J. and Damaren, C.J., State transition matrix optimization for formation flying reconfiguration maneuvers, unpublished manuscript.